Electronic Supplementary Material (ESI) for Journal of Materials Chemistry C.

Supporting Information

Thermochromism to Tune Optical Bandgap of a Lead-free Perovskite-type Hybrid Semiconductor for Efficiently Enhancing the Photocurrent Generation

Weichuan Zhang, Zhihua Sun, Jing Zhang, Shiguo Han, Chengmin Ji, Lina Li, Maochun Hong, Junhua Luo**

Contents

1. Experimental

Synthesis of ($C_{16}H_{20}N_2$)$SbBr_5$ A reaction mixture containing. 4-N,N-dimethylamino-4′-N′-methylstilbazolium iodide[1] (0.127g, 3.5 mmol) and Sb_2O_3 (0.11g, 3.0 mmol) in 20 mL 48% HBr by slow evaporation and illumination at room temperature. 4-N,N-dimethylamino-4-N-methylstilbazolium iodide, which was prepared from 4-picoline, Methyl iodide and 4-N,N-dimethylamino benzaldehyde in the presence of piperidine as catalyst. After several days later, bright bulk yellow crystals were obtained.

Material characterization: Raman and IR spectra Raman measurements were performed using a LabRAM HR confocal Raman system. The laser was focused through a 50× objective lens (NA = 0.7) with a spot size of ~500 nm. The excitation light source was a 532 nm laser with a power below 1 mW to avoid sample damage. The IR spectra data were collected by a Bruker Vertex 70 infrared spectrometer at room temperature.

Powder X-ray diffraction Powder X-ray diffraction (PXRD) for **1** was performed on a Miniflex600 X-ray diffractometer at different temperatures. The diffraction patterns were collected in the 2θ range of 5°−50° with a step size of 0.5°. The experimental power and film PXRD patterns obtained at room temperature, and simulated powder XRD pattern was acquired by the software of Diamond 3.2. Variable-temperature PXRD patterns were collected at 300 K, 350 K, 400 K, 450K and 500K on a D/MAX2500 Powder X-ray Diffractometer.

Dielectric constant measurements The pressed-powder pellets deposited with silver conducting paste were used for the dielectric constant measurements. The impedance analyses were performed on TongHui TH2828 analyzer in the temperature range from 130 to 410K, with an average heating/cooling rate of about 20 K/min.

Single-crystal structure determination A crystal (0.32 × 0.16 × 0.11 mm^3) was selected through an optical microscope for single-crystal XRD analysis. Single-crystal X-ray diffractions were performed on an Agilent SuperNova Dual diffractometer with an Atlas detector with a graphite-monochromatized Mo Kα radiation (λ = 0.71073 Å) at different temperatures. The collection of the intensity data, cell refinement, and data reduction were carried out with the program CrysAlisPro.[2] The structures were solved by the direct method with program SHELXS and refined with the least-squares program SHELXL.[3] The structures were verified using the ADDSYM algorithm from the program PLATON,[4] and no higher symmetries were found. Details of crystal parameters, data collection, and structure refinement are summarized in Table S1. The selected bond distances and angles are presented in Table S2. CCDC 1533611-1533615 contain the crystal data at the temperature 100K, 295K, 300K, 400K, 295K(red).

UV-vis-NIR Diffuse Reflectance Spectroscopy The UV-vis-NIR diffuse reflection data were obtained at room temperature and scan wavelength is between 200 nm and 1600 nm on a LAMBDA 950 UV/Vis Spectrophotometer. The BaSO4 powder sample was used as a standard (100% reflectance) and

Absorption (K/S) data were calculated from the following Kubelka-Munk function: K/S = (1–R)2 /2R, where R is the reflectance, K is the absorption, and S is the scattering. [5]

Computational Methods The first-principles calculations for 1 were performed by CASTEP [6] on a plane-wave pseudopotential total energy package based density functional theory (DFT). [7] The functional developed by Perdew-Burke-Emzerhoff (PBE) functional within the generalized gradient approximation (GGA) [8, 9] form was adopted to describe the exchange-correlation energy. The optimized norm-conserving pseudopotentials [10] in the Kleinman-Bylander [11] form for all the elements were used to model the effective interaction between atom cores and valence electrons. The calculated mode was optimized with a k-point sampling of 3 × 3 × 3 and cutoff energy of 820 eV. The other parameters and convergent criteria were the default values of CASTP code.

Photoconductivity measurement The dispersed solutions of 1 were used to assemble thin-films using spin-coating method as the Schematic diagram of Au device architecture shows in figure. 4a. Current-voltage curves of the device performed by a Model 6517B Electrometer with a ST-102D Probe station. the light data was obtained under a light source with a 300mWcm^{-2} Xenon lamp at room temperature. The response time of current was operated at a bias voltage of 5V and an incident power of 100 μW mm^{-2} 520 nm laser in National Laboratory for Infrared Physics, Shanghai Institute of Technical Physics, Chinese Academy of Sciences, Shanghai 200083, China.

AFM and C-AFM measurement The AFM and Conductive AFM (C-AFM) measurements were performed using a Bruker Dimension Icon system. C-AFM was performed using a Veeco Nanoscope V instrument equipped with a peak force-TUNA module. Budget Sensors PFTTUNA probes were used, and a +10 V sample bias was applied during each scan. For height sensor-mode imaging, Budget Sensors 0.4N/m SCMASYST-air was used.

Differential scanning calorime measurements The differential scanning calorime of 1 were performed using a NETZSCH DSC 200 F3 DSC instrument in the temperature range of 0-100 °C for seven cycle times. The crystalline samples were placed in aluminum crucibles that were heated and cooled with a rate of 20 K/min under the nitrogen atmosphere.

2. Figures

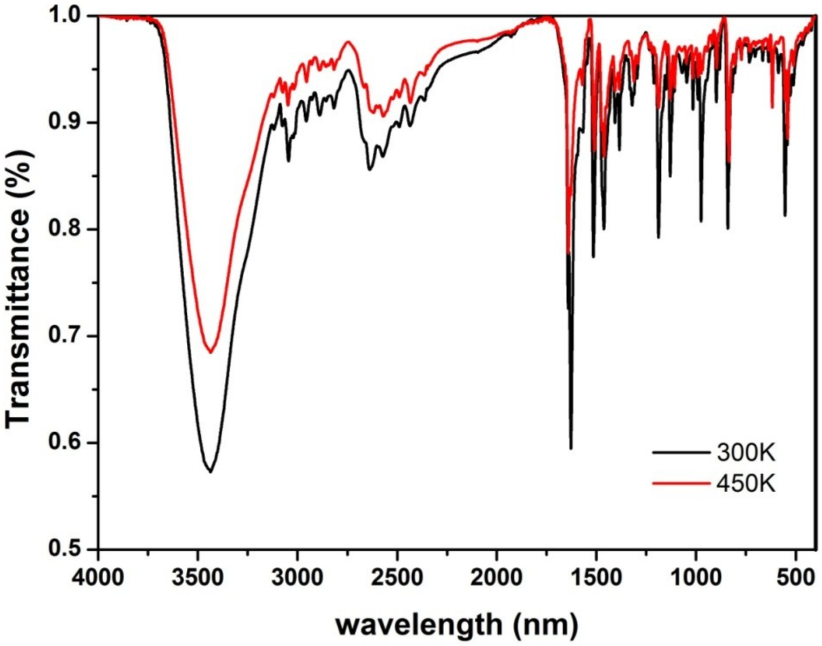

Figure S1. The 300 and 450K-crystal **1** was characterized by infrared spectroscopy at room temperature. The results showed that the cation in **1** was stable

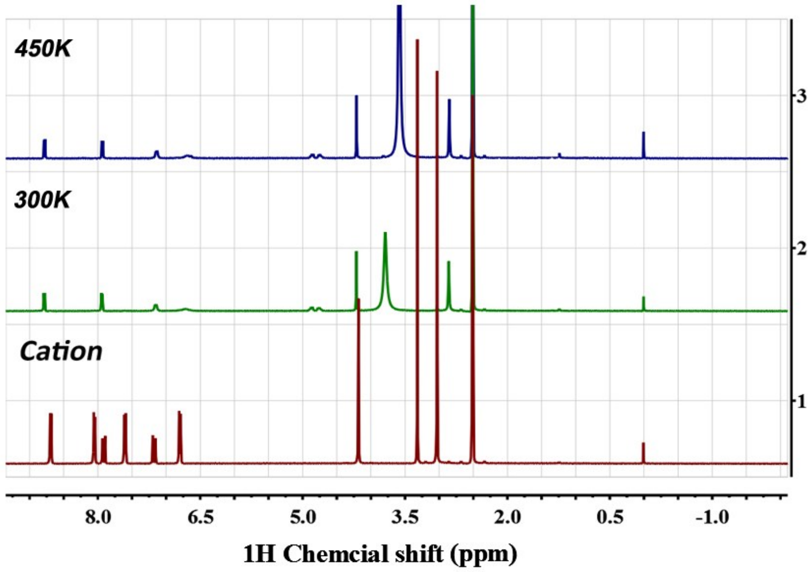

Figure S2. The ^{1}H NMR spectra of 300K and 400K crystal that dissolved in dimethyl sulfoxide-d6 and characterized at room temperature. It shows that complex **1** was pure and stabilization in the temperature range from 300 to 450K.

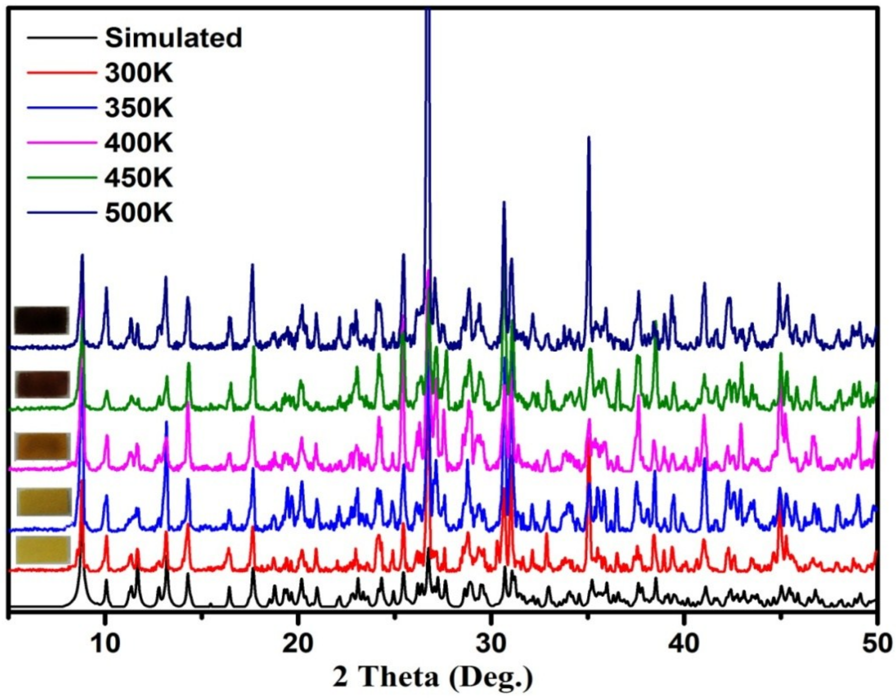

Figure S3. Variable-temperature PXRD patterns of **1** showing the structural without phase transition in the temperature range 300–500 K. The color-changed power were displayed at bottom-left corner near theirs PXRD patterns.

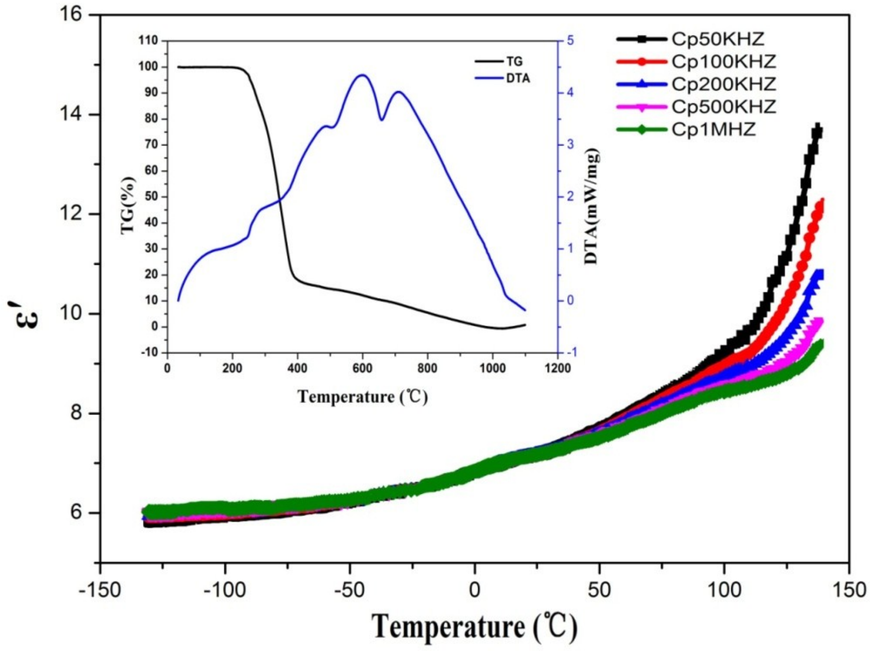

Figure S4. Temperature-dependent dielectric constants of 1 at different frequencies. The thermogravimetric analysis and differential thermal analysis were displayed at upper-left corner. Dielectric measurement is treated as an effective indicator of structural phase transition. Here, the bulk crystal 1 was applied to the dielectric measurements between 140 K and 420 K and the dielectric constant (ε′) remains stable with a quite small rise without phase transition. Thermogravimetric analysis and differential thermal analysis showed that this material is stable up to 426 K and no phase transitions within this temperature range.

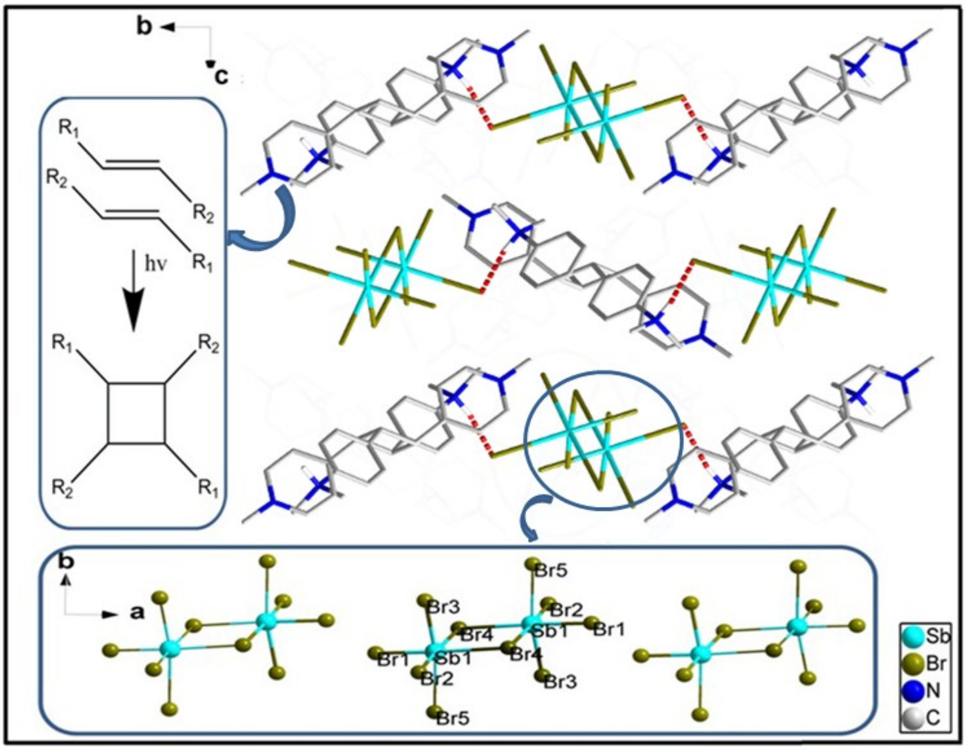

Figure S5. Stacking structure along the a-axis and view of the 1D-like structure formed by stibonium and bromide ion, H atoms are omitted for clarity.

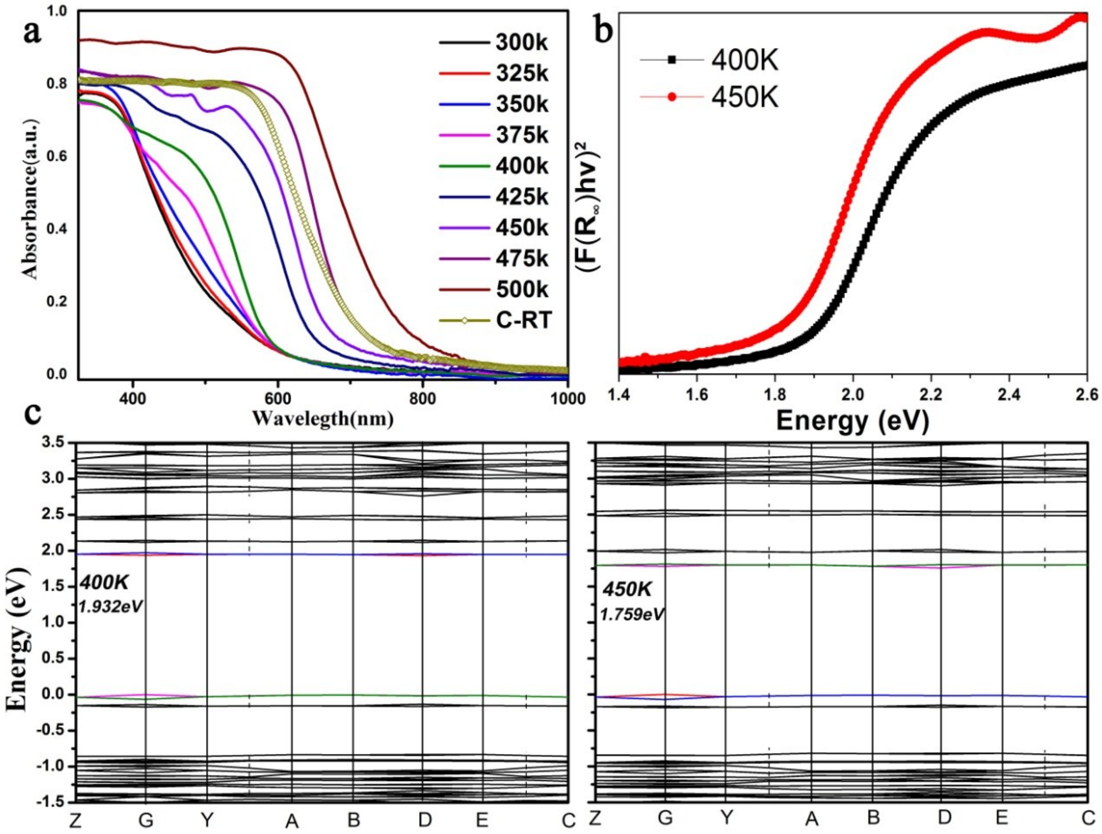

Figure S6. (a)Ultraviolet-vis absorption spectra of 1 performed on sample preheated at different temperatures, (b) the ab Tauc plot, and(c), (d) calculated band structure of 1at 400 and 450K.

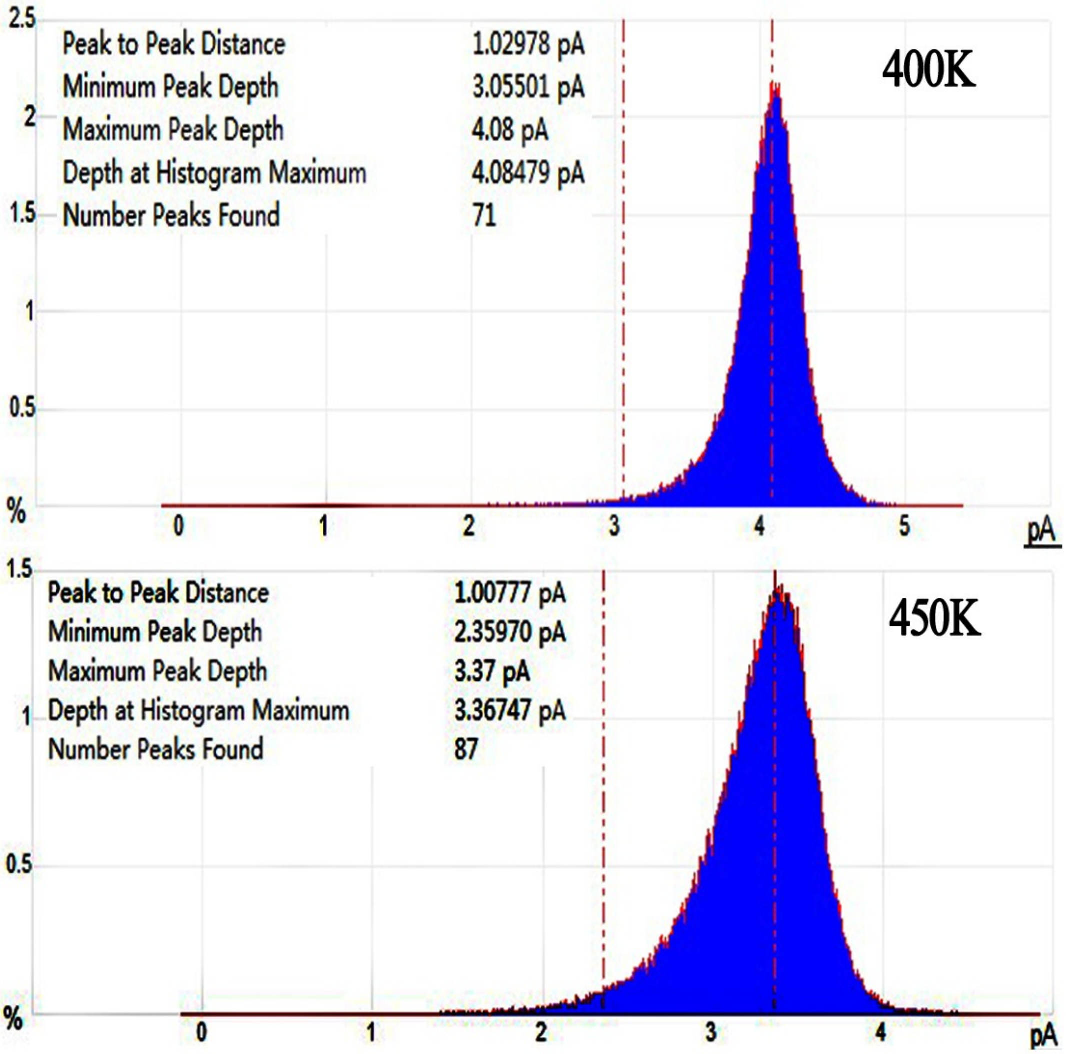

Figure S7. The data histograms of conductive AFM were recorded in the same film at 400K and 450K.

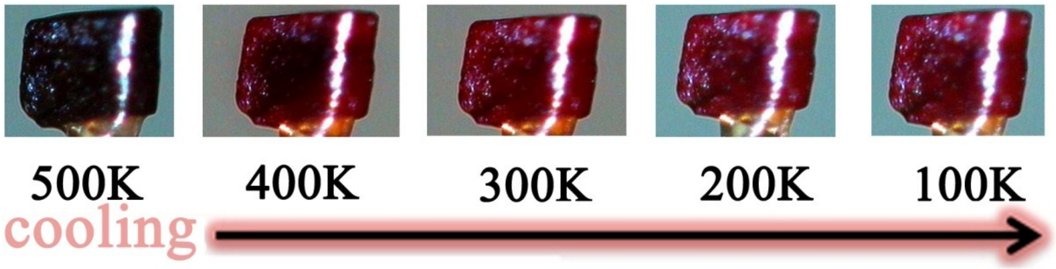

Figure S8. Thermochromism induce color changed in the temperature range from 500K to100K.

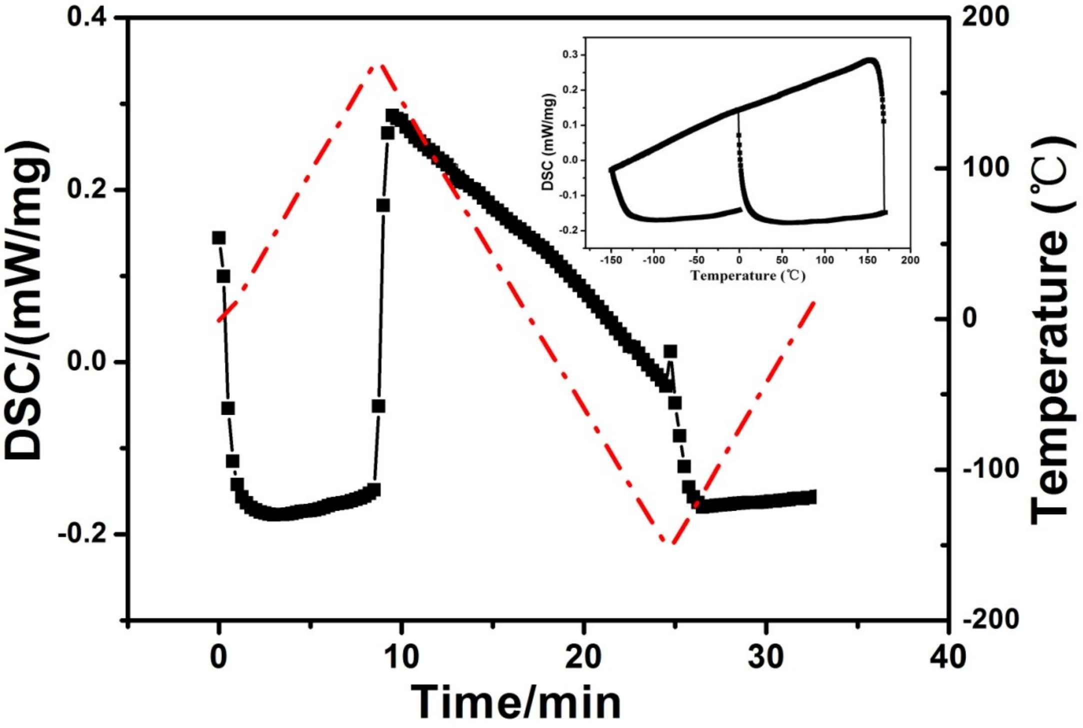

Figure S9. The differential scanning calorimetry of **1**.

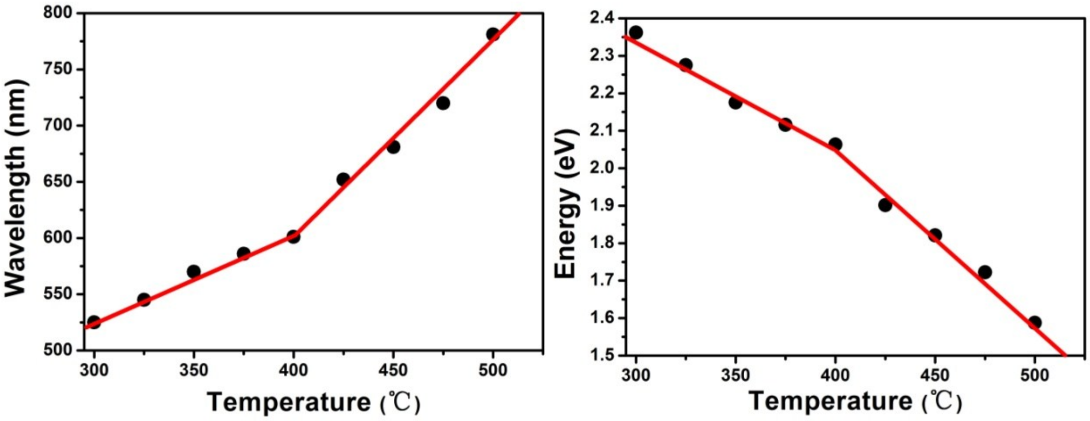

Figure S10. Temperature dependent of band edge change and absorption spectra during the melting process.

3. Tables

Table S1. Crystal data for **1** at different temperatures.

Empirical formula	$C_{16}H_{20}Br_5N_2Sb$				
Identification code	100K	295K	300K	400K	450K
Formula weight	761.64	771.65	761.64	761.64	763.64
Temperature/K	100 (4)	295(2)	300 (10)	400 (10)	295 (10)
Crystal system	monoclinic	monoclinic	monoclinic	monoclinic	monoclinic
Space group	$P2_1/n$	$P2_1/n$	$P2_1/n$	$P2_1/n$	$P2_1/n$
a/Å	10.7852(7)	10.9363(9)	10.9541(3)	11.0102(6)	10.9137(5)
b/Å	15.1260(7)	15.1310(10)	15.1744(4)	15.1858(8)	15.1660(6)
c/Å	13.5099(8)	13.6064(9)	13.6577(4)	13.6416(9)	13.6160(5)
α/°	90	90	90	90	90
β/°	100.220(6)	99.786(8)	99.732(3)	99.313(6)	99.598(4)
γ/°	90	90	90	90	90
Volume/Å^3	2169.0(2)	2218.8(3)	2237.54(11)	2250.8(2)	2222.15(15)
Z	4	4	4	4	4
ρ_{calc}g/cm^3	2.332	2.31	2.261	2.248	2.283
μ/mm^{-1}	10.485	10.25	10.164	10.104	10.236
F(000)	1424.0	1444	1424	1424	1428
Radiation (MoKα)	0.71073	0.71073	0.71073	0.71073	0.71073
2Θ range for data collection/°	6.616 to 57.004	6.974 to 58.86	6.956 to 58.916	6.954 to 59.452	6.97 to 59.134
Index ranges	-14≤ h≤ 9 -19≤k≤17 -16≤ l≤18	-14≤h≤15 -20≤k≤20 -18≤l≤14	-14≤h≤14 -20≤k≤20 -17≤l≤18	-12≤h≤15 -20≤k≤17 -16≤l≤17	-13≤h≤15 -20≤k≤19 -18≤l≤18
Reflections collected	12449	14667	15126	15239	14983
Independent reflections	5005 [R_{int} = 0.1158, R_{sigma} = 0.1210]	5290 [R_{int} = 0.0439, R_{sigma} = 0.0543]	5425 [R_{int} = 0.0346, R_{sigma} = 0.0455]	5576 [R_{int} = 0.0869, R_{sigma} = 0.1268]	5345 [R_{int} = 0.0306, R_{sigma} = 0.0456]
Data/restraints/parameters	5005/0/220	5290/0/220	5425/0/220	5576/1/253	5345/0/220

Goodness-of-fit on F^2	0.999	1.018	1.026	1.028	1.017
Final R indexes [I>=2σ (I)] R_1[a] &wR_2[b]	R_1 = 0.0665, wR_2 = 0.1561	R_1 = 0.0378, wR_2 = 0.0793	R_1 = 0.0395, wR_2 = 0.0786	R_1 = 0.0887, wR_2 = 0.1812	R_1 = 0.0362, wR_2 = 0.0554
CCDC NO.	1533611	1533612	1533613	1533614	1533615

[a] $R(F_o) = \sum||F_o| - |F_c||/\sum|F_o|$. [b] $R_w(F_o) = (\sum_w||F_o| - |F_c||^2/\sum|F_o|^2)^{1/2}$, $w = [\sigma^2(F_o) + (0.002F_o)^2]^{-1}$

Table S2. Selected bond lengths (Å) for **1** at different temperatures.

Bond	**Bond length**				
	100K	295K	300K	400K	295k(450K)
Sb1-Br1	2.5983	2.6144	2.6076	2.6080	2.6045
Sb1-Br2	2.7220	2.7273	2.7293	2.710	2.7097
Sb1-Br3	2.6572	2.6322	2.6632	2.6471	2.6391
Sb1-Br4	2.9316	2.9261	2.9478	2.938	2.9297
Sb1-Br5	3.0651	3.0722	3.0798	3.0835	3.0792

The crystallographic data, CCDC number and experimental details for the structural analyses of complex **1** in this paper are summarized in Table S1. Here, we used a formula C=R/V to explain thermochromism in figure 2b, where C is rate of bond change, R is bond length, and V is the volume of crystal cell. Fortunately, this method are well fit with our data and easily to reflect change law(figure 2b).

4. References

[1] Z. Sun, J. Luo, T. Chen, L. Lina, R.-G. Xiong, M.-L. Tong and M. Hong, *Adv. Funct. Mater.*, 2012, **22**, 4855.

[2] CrysAlisPro, Version 1.171.36.28, *Agilent Technologies: Santa Clara*, CA, 2013.

[3] G. M. Sheldrick, *Acta Crystallogr. A*, 2008, **64**, 112.

[4] A. L. Spek, J. *Appl. Crystallogr*., 2003, **36**, 7.

[5] Tauc. Absorption edge and internal electric fields in amorphous semiconductors. *J. Mater. Res. Bull.*, 1970, **5**, 721.

[6] S. J. Clark, M. D. Segall, C. J. Pickard, P. J. Hasnip, M. J. Probert, K. Refson and M. C. Payne, First principles methods using CASTEP. *Z. Kristallogr. - Cryst. Mater*, 2005, *220*, 567.

[7] M. C. Payne, M. P. Teter, D. C. Allan, T. A. Arias and J. D. Joannopoulos, *Rev. Mod. Phys*,. 1992, **64**, 1045.

[8] D. M. Ceperley and B. J. Alder, Ground-state of the electron-gas by a stochastic method. *Phys. Rev. Lett.*, 1980, **45**, 566.

[9] J. P. Perdew and A. Zunger, Self-interaction correction to density-functional approximations for many-electron systems. *Phys. Rev. B: Condens. Matter Mater. Phys.*, 1981, **23**, 5048.

[10] A. M. Rappe, K. M. Rabe, E. Kaxiras and J. D. Joannopoulos, *Phys. Rev. B: Condens. Matter Mater. Phys.*, 1990, **41**, 1227.

[11] L. Kleinman and D. M. Bylander, Efficacious form for model pseudopotentials. *Phys. Rev. Lett.* 1982, **48**, 1425.